

Evaluation of Bulk and Surfaces Absorption Edge Energy of Sol-Gel-Dip-Coating SnO₂ Thin Films

Emerson Aparecido Floriano^a, Luis Vicente de Andrade Scalvi^{a,b,*},

Julio Ricardo Sambrano^c, Viviany Geraldo^{b,d}

^aAdvanced Materials Group & Defects in Semiconductors and Insulators Group, State University of São Paulo – UNESP, CP 473, CEP 17033-360, Bauru, São Paulo, Brazil

^bDepartment of Physics – FC, State University of São Paulo – UNESP, CP 473, CEP 17033-360, Bauru, São Paulo, Brazil

^cModeling and Molecular Simulation Group – DM / FC, State University of São Paulo – UNESP, CP 473, CEP 17033-360, Bauru, São Paulo, Brazil

^dLaboratory of Nanomaterials, Federal University of Minas Gerais – UFMG, CEP 31270-901, Belo Horizonte, MG, Brazil

Received: February 12, 2010; Revised: October 20, 2010

The absorption edge and the bandgap transition of sol-gel-dip-coating SnO₂ thin films, deposited on quartz substrates, are evaluated from optical absorption data and temperature dependent photoconductivity spectra. Structural properties of these films help the interpretation of bandgap transition nature, since the obtained nanosized dimensions of crystallites are determinant on dominant growth direction and, thus, absorption energy. Electronic properties of the bulk and (110) and (101) surfaces are also presented, calculated by means of density functional theory applied to periodic calculations at B3LYP hybrid functional level. Experimentally obtained absorption edge is compared to the calculated energy band diagrams of bulk and (110) and (101) surfaces. The overall calculated electronic properties in conjunction with structural and electro-optical experimental data suggest that the nature of the bandgap transition is related to a combined effect of bulk and (101) surface, which presents direct bandgap transition.

Keywords: tin dioxide, sol-gel, thin films, electronic structure, optical absorption

1. Introduction

Electronic ceramics have received a great deal of attention in the past 10 years, in the seeking for technological innovation^{1,2}. These ceramics usually are composed of metallic oxides, and play very important role as catalytic, solar cells, capacitors, gas sensors, varistors, among others³. Electrical and optical properties of this class of materials are strongly dependent on the final microstructure, which can be controlled by composition and chemical nature of doping, grain size and temperature of thermal annealing. Among the electronic ceramics, tin dioxide (SnO₂) deserves special attention due to its potentialities in optoelectronics devices. This compound has tetragonal structure of rutile type and may be characterized as an n-type semiconductor with wide bandgap, in the range 3.6-4.0 eV. It presents high transparency in the visible range and high reflectivity in the infrared⁴. Its processing normally gives birth to defects such as oxygen vacancies and interstitial tin atoms, which act as donors in the SnO₂ matrix, increasing the electron density in the conduction band, explaining the n-type conduction. Then, even in the undoped form, tin dioxide presents fair n-type electrical conductivity⁵. The preferential direction of SnO₂ growth is an important parameter related to its structure and then to its electrical conductivity. These characteristics are influenced by the method of thin film deposition, molar concentration of the starting solutions, time and temperature of thermal annealing⁶.

The SnO₂ band structure diagram has been a motive of controversy among published literature, involving either experimental as well as theoretical papers. Some papers point to a direct bandgap transition^{7,8} whereas others indicate indirect bandgap^{9,10}. The complexity of tin dioxide electronic structure makes difficult the precise determination of the bandgap transition nature¹¹. Optical absorption measurements allow estimation of the bandgap transition around the fundamental absorption edge, besides they give indications about its nature¹².

The electrical conductivity of layers prepared by the sol-gel-dip-coating process is lower compared to films deposited by other techniques. This performance is generally attributed to a combination of effects associated to nanosized grains of sol-gel materials. As shown in this paper, crystallites generated by our sol-gel dip-coating route have nanoscopic dimensions. Therefore a considerable amount of crystallites is present in the material, which makes electron scattering at grain boundaries the most relevant mechanism to the film conductivity^{13,14}. The physics of electronic conduction in these films is peculiar and rather unknown. Therefore, it deserves a careful investigation.

Under a theoretical point-of-view, computational simulation based on periodic first principles calculations has demonstrated great relevance in the evaluation of electronic structure of crystalline solids. The simulation leads to prediction of structure and electronic properties of solids, either qualitative as well as in a quantitative way^{15,16}. Besides, it may yield properties hard or even impossible to measure experimentally. Electronic structure of bulk and SnO₂ surfaces affect directly optical, structural and electric properties of the material^{6,17}. Among the several surfaces of SnO₂, the (110) surface deserves special attention, because it is thermodynamically and electrostatically the most stable, even though the faces (101) and (011) are also relevant. The surface (110) presents the least surface energy when compared to other material surfaces¹⁸. Its structure consists of planes containing the oxygen and tin atoms separated by planes containing only oxygen atoms. This sequence may be summarized as follows: O – Sn₂O₂ – O – O – Sn₂O₂ – O, etc, with ionic charges 2⁻, 4⁺ and 2⁻¹⁹. This surface is the most investigated, either experimentally as theoretically, mainly concerning the identification of atomic species present in the surface^{20,21}. Band structure calculation, performed through the Tight Binding method²² or Density functional theory¹⁷ points to the bandgap transition of (110) surface as having indirect nature.

*e-mail: scalvi@fc.unesp.br

Another important face of SnO_2 is the (101) surface, because it is the dominant in materials with nanoscopic dimensions²⁰, presenting potential application in nanostructured wires²³.

In this work, we present results concerning the electrical transport in nanocrystalline undoped SnO_2 thin films. Photocurrent spectra are obtained by using a deuterium source to irradiate the sample in the ultraviolet range, at low temperature. In order to have the photoconductivity response of these films, spectra must be normalized, concerning the film optical absorption and the photon flux reaching the sample. The net result is the photoconductivity quantum yield, which shows marked temperature dependence¹⁴. The aim in this paper is to use the photocurrent spectra to determine the absorption coefficient as function of temperature and then, evaluate the bandgap transition energy. This paper also aims to bring on a correlation between theoretical and experimental approaches. The main goal is to evaluate experimentally structural and optical properties of SnO_2 thin films and compare with theoretical results obtained by the Density functional theory, applied to periodic models. This theoretical treatment is used to investigate the electronic properties of bulk and (110) and (101) surfaces, concerning the band energy diagram. These results are discussed and compared with X-ray diffraction, optical absorption and photoconductivity measurements in the ultraviolet-visible range.

2. Experimental Approach

Colloidal suspensions of undoped SnO_2 have been prepared through the sol-gel route, from solutions with distinct molar concentrations, which are called here method I and method II. Firstly, it has been prepared an aqueous solution of $\text{SnCl}_4 \cdot 5\text{H}_2\text{O}$ (0.5 M). Under stirring with a magnetic bar, NH_4OH was then added until the pH reaches 11, leading to hydrolysis and condensation reactions. The remaining precipitated was submitted to dialysis against distilled water for proximately 10 days, in order to eliminate Cl^- and NH_4^+ ions. This procedure leads to a stable and transparent suspensions (sol) of SnO_2 with a volume increase of about 10 times (due to the dialysis process). This is called method I and its final concentration is 0.05M. The suspension obtained by the method I was then heated to 100 °C, until the dispersant agent (water) had 70% of this initial

volume eliminated by evaporation. This procedure leads to a more viscous solution with final concentration of 0.2 M. This suspension is called method II. Thin films are deposited by the dip-coating technique on quartz substrates, starting from suspension obtained by method I and II. Quartz substrates are very important tool, since this material has absorption edge wavelength rather below the SnO_2 absorption edge (about 350 nm), which do not mask the ultraviolet spectra of films deposited on this sort of substrates. Substrates are vertically dipped into the suspension with dipping rate of 10 cm/min. Films were fired at 400 °C by 10 minutes, between each layer. The total number of layers was 30 by the film obtained by method I and 10 for the film deposited by method II. Both samples have a final annealing at 550 °C, at room pressure conditions, for 1 hour. Resulting thickness in both cases is about 300 nm, as obtained by scanning electron microscopy (SEM) of cross section.

X-ray diffraction data of films were obtained with a RIGAKU diffractometer, model D/MAX-2100/PC, coupled with a $\text{Cu K}\alpha$ (1.5405 Å) radiation source and a Ni filter for elimination of $\text{K}\beta$ radiation. Scanning rate was 1 degree/minute in the range 20 to 80°. Optical absorbance was carried out in a Cary spectrophotometer, in the range 190 to 900 nm (ultraviolet to near infrared). Photocurrent spectra are obtained by using a deuterium source (30 W) to irradiate the sample in the ultraviolet range, through a computer controlled Oriel ultraviolet monochromator and holographic diffraction grating. The photocurrent was continuously recorded with a 6517A Keithley electrometer. The low temperature is obtained by using a closed cycle helium cryostat of APD-Criogenics and a Lake Shore temperature controller, with a 0.05 degree of precision.

3. Theoretical Method and Model System

SnO_2 crystallizes in tetragonal rutile structure and belongs to the space group $\text{P}4_2/\text{mnm}$. The structure of the conventional rutile unit cell of SnO_2 is characterized by two lattice parameters, a and c , (Figure 1a) and an internal parameter u associated with the O atomic position. There are two formula units per primitive unit cell; with the threefold-coordinated oxygen atoms forming distorted octahedral configurations around the Sn atoms.

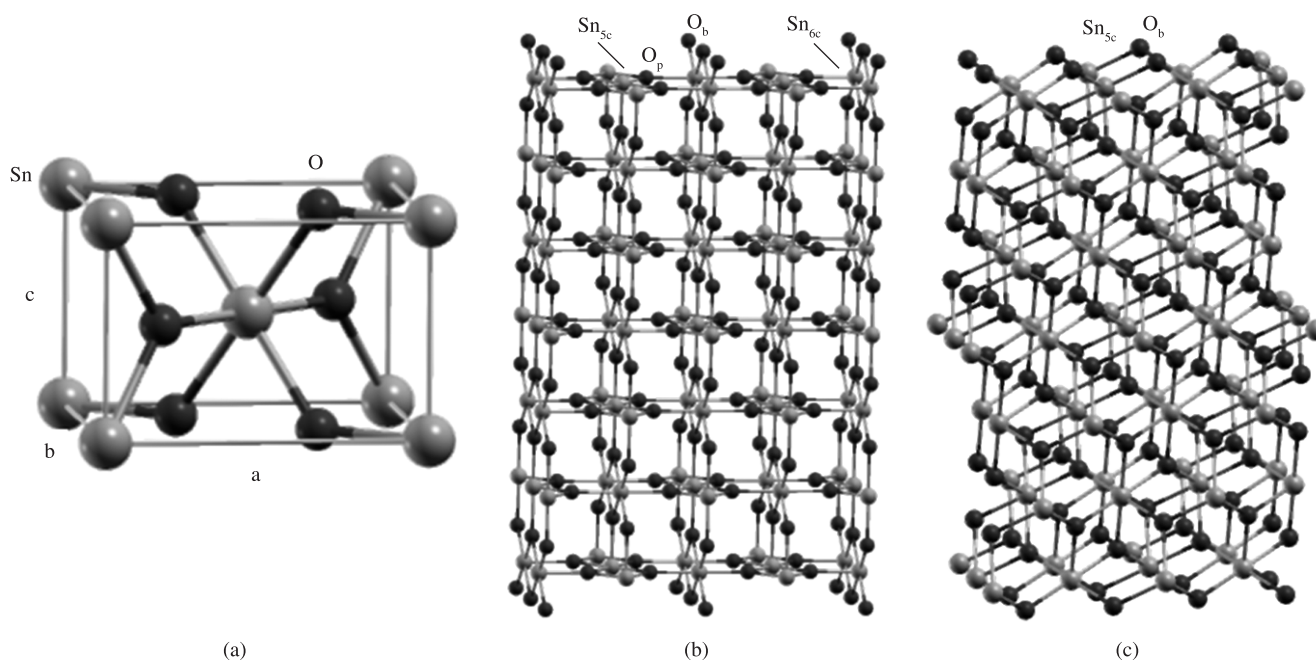


Figure 1. a) Rutile tetragonal unit cell; b) (110) surface structure; and c) (101) surface structure.

A periodic first-principle calculation, based on density functional theory (DFT)²⁴ with the Becke's three-parameter hybrid nonlocal exchange function²⁵, combined with the Lee-Yang-Parr gradient-corrected correlation function²⁶, B3LYP, were performed by using the CRYSTAL06 computer code²⁷. This functional have yielded results comparable to more sophisticated correlated calculations or perturbation models²⁸ and have been employed successfully in studies on the electronic and structural properties of the bulk and surfaces of several systems²⁹⁻³¹.

The atomic centers have been described by DB-31G³² for O atom and DB-21G³³, for Sn atom, where DB refers to Durand-Barthelat non-relativistic large effective core potential³⁴. The experimental values of the lattice constant are: $a = 4.737 \text{ \AA}$, $c = 3.186 \text{ \AA}$ ^[35], and $u = 0.306$ ^[35]. From these parameters, we have carried out the optimization procedure, yielding: $a = 4.702 \text{ \AA}$, $c = 3.194 \text{ \AA}$ and $u = 0.306$. Our results are only $\sim 0.01\%$ lower than the experimental data for the a parameter, $\sim 0.01\%$ larger for the c parameter and 0% for the internal parameter u. These results are in good agreement with other theoretical and experimental data^{17,18,35}.

From this optimized parameters, two surfaces structures (110) and (101) have been modeled, by taking into account the mirror symmetry with respect to the central layers, slab models. These slabs are finite in the c-direction but periodic in a- and b-directions. Both slabs are depicted in Figure 1.

In order to select the size of the slab models, we have calculated the surface energy by using 9 to 21 layers. These energies have converged to its infinite thickness. Thus, 21 layers may be sufficient to describe the surface geometry for both surfaces.

The (110) termination results in an outermost plane of oxygen atoms that appears in rows along the [001] direction (Figure 1b). These O atoms are called "bridging" (O_b) atoms. In the second atomic layer, there are fivefold-coordinated (Sn_{5c}), and sixfold-coordinated (Sn_{6c}) Sn atoms and O atoms in the same plane (O_p). A third and fourth plane of oxygen atoms are located below that. The SnO₂ surface (101) consists of fivefold-coordinated Sn (Sn_{5c}) atoms and of alternating rows of twofold-coordinated O (O_{2c}) atoms and threefold coordinated O (O_{3c}) atoms, situated slightly below the plane of the Sn atoms³⁶.

The effect of relaxation has been analyzed on the (110) and (101) surfaces by fully relaxation of all atoms, i.e., the O and Sn atoms are free to move along x-, y- and z-directions. The results are presented in Table 1.

The positive displacements in z-direction, Δz , denote relaxations toward the vacuum region and the negative displacement indicate relaxations inward the bulk. For SnO₂ (110) surface the displacements of the O_b, 0.01 Å, O_p, 0.11 Å and Sn_{6f}, 0.2 Å in the z-direction are toward the vacuum region and the Sn_{5f} inward the bulk. The relaxation of the (101) surface show that the O_b and Sn_{5f} are displaced toward the vacuum by 0.03 and 0.02 Å, respectively. Our results are in a similar range that previous reported data of Beltran and other theoretical results^{37,38}. The displacement of the Sn atoms are larger than the oxygen atoms, leading a rumpling of the layers.

Table 1. Atomic displacements, Δx , Δy and Δz (Å), for the (110) and (101) surfaces.

	(110) surface				(101) surface	
	O _b	Sn _{5f}	Sn _{6f}	O _p	O _b	Sn _{5f}
Δx	0.0	0.0	0.0	0.0	0.06	0.13
Δy	0.0	0.0	0.0	-0.05	0.0	0.02
Δz	0.01	-0.12	0.2	0.11	0.03	0.02

Experimental and theoretical analysis indicates that the (110) surface is the most stable of the rutile structure with the lowest surface energy^{18,21,37,39}. The surface stability order is (110) < (010) < (101) < (001)³⁹.

The XCRYSDEN program⁴⁰ has been used for design of band structure of bulk and surfaces. The band structures were obtained for 80 \vec{K} points along the appropriate high-symmetry paths of the adequate Brillouin zone.

4. Results and Discussion

4.1. Structural properties

Figure 2 shows X-ray diffraction data for films of SnO₂ prepared respectively by methods I and II. It is easily verified that films present rutile type structure⁴¹. It is indicated in Figure 2 the cassiterite phase main directions as well as the crystallite size (t) calculated according to the Scherrer equation⁴². It also can be verified in Figure 2 that the thin film prepared through method II (more viscous solution) presented strong intensity in the direction (101) related to directions (110) and (211). The thin film prepared by the method I (less viscous solution) presented strong intensity in the (101) and (110) directions, however the peak is slightly more intense for (101) direction than the peak for direction (110). The smaller number of layers leads to less interface defects and then a cleaner diffractogram is expected, as verified in figure 1 for the method II thin film (10 layers), where the cassiterite phase structure is much better defined.

In order to evaluate the preferential growth direction, the texture coefficient (CT) of samples is calculated by relating the relative intensity of the diffraction peaks with a random oriented sample (reference sample). JCPDF data⁴¹ was used for peak identification. CT is the preferential growth of crystalline plans parallel to film surface, and has been calculated by Equation 1^[43]:

$$CT = N \frac{I(hkl)/I_0(hkl)}{\sum_1^N I(hkl)/I_0(hkl)} \quad (1)$$

where $I(hkl)$ are the intensities of X-ray diffraction peaks of investigated samples, $I_0(hkl)$ are the intensities of X-ray diffraction

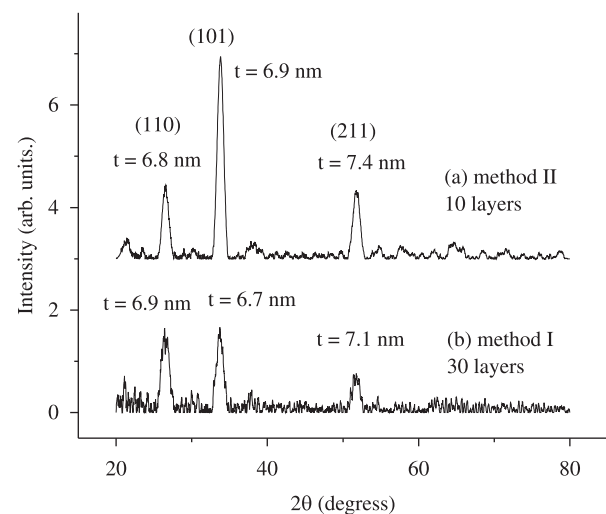


Figure 2. X-ray diffractogram for undoped SnO₂ thin film. a) Obtained by method II – 10 layers and b) obtained by method I – 30 layers. The three mean directions are indicated along with the evaluated crystallite size.

peaks of a polycrystalline material with random orientation (reference) and N is the number of analyzed peaks in the diffractogram. CT close to 1 (one) indicates a non-texturized material, and CT close to N indicates a higher texturization.

Table 2 brings the calculated values of CT , according to Equation 1, for the (hkl) crystallographic plans and relative intensities, associated with the experimental data of X-rays diffraction of films prepared by methods I and II, presented in Figure 2, as well as the reference (JCPDS – 41-1445)⁴¹.

As can be seen in Table 2, calculation of CT indicates that the SnO_2 thin film presents the (101) direction as preferential for the growth. Besides the film prepared by the method II (more viscous suspension) presents a higher CT in this direction, compared to film prepared using method I (less viscous suspension).

4.2. Optical absorption

Optical absorption coefficient (α) may be evaluated from absorbance data, when the material thickness is known. Scanning electron microscopy of cross section (not shown) yields the thickness as about 300 nm. From the evaluation of α , the material bandgap may be estimated by using the Equation 2⁴⁴:

$$(\alpha h\nu)^{2/y} = A^* (h\nu - E_g) \tag{2}$$

where α is the absorption coefficient, A^* is a constant, y is an integer, that defines the sort of transition, for $y=1$ (direct transition) and $y=4$ (indirect transition). The energy magnitude is determined by extrapolation for the linear range of the experimental curve $(\alpha h\nu)^2$ to x axis.

Figure 3 represents the optical absorption spectra of SnO_2 thin film, deposited on quartz substrates, produced by the method II. The inset of Figure 3 shows the bandgap evaluation of this material, assuming that the band transition is direct. It is important to mention again that the use of quartz substrates is fundamental for investigating optical properties of SnO_2 , because the quartz absorption does not coincides with the tin dioxide absorption edge, avoiding masking the bandgap evaluation⁴⁴. From Figure 3 it is verified that the material bandgap is about 4.1 eV, in good agreement with published data^{45,46}.

4.3. Relationship between photoconductivity and optical absorption

When radiation is shined on a semiconductor sample with electrical conductivity σ , the fraction of the incident radiation after propagation through a distance x , is given by Equation 3⁴⁷:

$$\frac{P(x)}{P(0)} = \exp(-\alpha \cdot x) \tag{3}$$

where α , the absorption coefficient, is given by Equation 4⁴⁷:

$$\alpha = \frac{4\pi\nu k}{c} \tag{4}$$

where k is the imaginary part of the refraction index, called extinction coefficient.

From Maxwell equations, after a straightforward algebra, it may be concluded that (Equation 5):

$$nk = \frac{\sigma}{\nu} \tag{5}$$

Combination of Equations 4 and 5 yield a relation between absorption coefficient (α) and electrical conductivity (σ) (Equation 6):

$$\alpha = \frac{4\pi\sigma}{nc} \tag{6}$$

Table 2. Texture coefficients (CT) for SnO_2 thin films.

Reference*	SnO_2 – Method I		SnO_2 – Method II	
(hkl)	I/I_o	CT	I/I_o	CT
(110)	1	0.98	0.34	0.45
(101)	0.75	1	1	1.77
(211)	0.57	0.46	0.33	0.79

*(JCPDS – 41-1445).

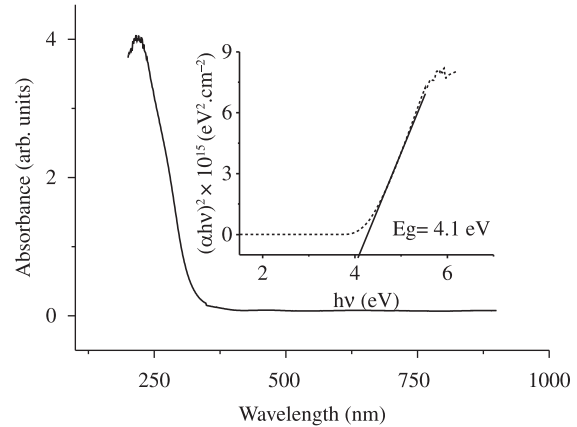


Figure 3. Optical absorption spectra for undoped SnO_2 thin film. Inset – experimentally obtained direct bandgap, through extrapolation of linear range of $(\sigma h\nu)^2$ for $y=0$.

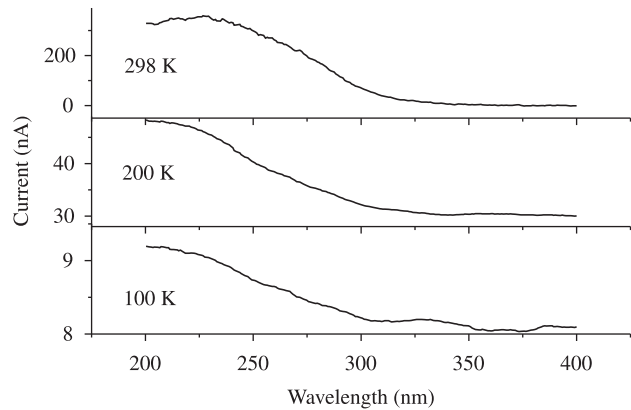


Figure 4. Excitation of photoconductivity spectra for SnO_2 thin film, obtained at distinct temperatures.

Equation 6 may be used to evaluate the semiconductor bandgap from photo-induced electrical conductivity spectra data, where the conductivity is monitored by the wavelength of irradiating light. Figure 4 shows photoconductivity spectra data, measured for some distinct temperatures. It is easily verified that as the temperature decreases, the overall magnitude of photo-induced current also decreases. This is expected because the resistivity is supposed to increase as the film cools down, a typical semiconductor behavior. Moreover, the optical signal reaching the sample is rather low and does not promote a high free carrier excitation, which means that the resistivity follows the same shape of the dark conductivity. To obtain a normalized photoconductivity spectrum, it is important to calculate photoconductivity quantum yield¹⁴, where the measured photocurrent is normalized by the photon flux in order to eliminate the dependence of the excitation upon the incident light intensity

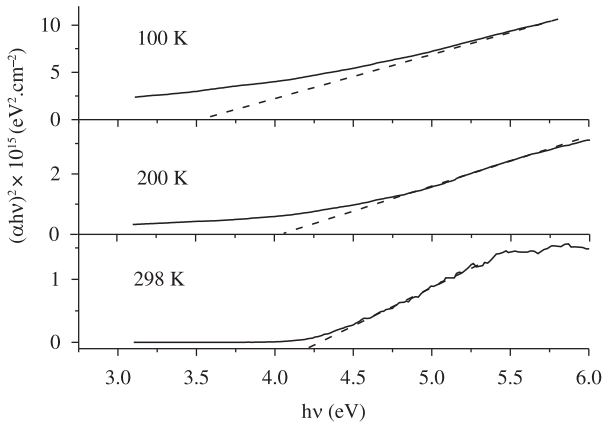


Figure 5. Direct bandgap evaluation using photoconductivity data for SnO₂ thin film, obtained at distinct temperatures.

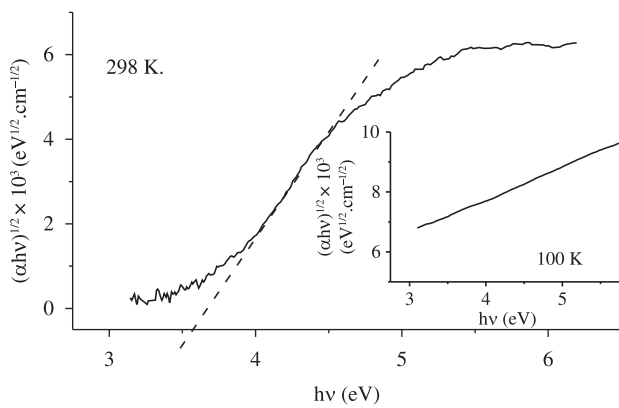


Figure 6. Indirect bandgap evaluation using photoconductivity data for SnO₂ thin film, at room temperature. Inset: Attempt to evaluate indirect bandgap at 100 K.

and sample absorption coefficient. This procedure can be seen elsewhere¹⁴ but it is not the scope of this paper. Transforming the electrical photoconductivity data in absorption coefficient, according to Equation 6, the bandgap transition can be evaluated. Figure 5 shows the determination of band gap energy by considering direct band transition. The value obtained for room temperature, 4.2 eV, is about the same value obtained for evaluation directly from optical absorption data. For 200 K, E_g decrease to 4 eV and for 100 K, E_g is 3.5 eV. Decrease of band gap energy with cooling down is an expected result, because it is a typical behavior of well known semiconductor such as Si and Ge⁴⁸. However the temperature variation rate obtained here is rather high. Absorption coefficient as function of temperature measurements are under progress and will rule as a comparison parameter for our estimation. A more complete approach where the normalization is taken into account may be important to determine the precision of band gap evaluation through photoconductivity data. On the other hand, by considering indirect transition, as shown in Figure 6, only the evaluation of room temperature band gap is possible. When the temperature is decreased, the evaluation of the band gap energy becomes impossible through this procedure, because the extrapolation for the abscissa crossing $((\alpha h\nu)^{1/2} = 0)$ leads to negative values. We may conclude that, although the band gap variation with temperature is rather high, the application of the band gap evaluation from temperature dependent photoconductivity data works much better when direct band gap transition is assumed.

4.4. Bulk and surface band structure diagram

Figure 7a and b represents the band structures of the bulk SnO₂, and appropriate high-symmetry paths of the adequate Brillouin zone. The points of the Brillouin zone, chosen in our procedure, are the same used by Robertson⁸. The top of valence band (VB) is located at Γ point. The gap is direct, 3.55 eV, in accordance to the experimental optically measured gap^{45,46} and other theoretical works^{18,37,49}.

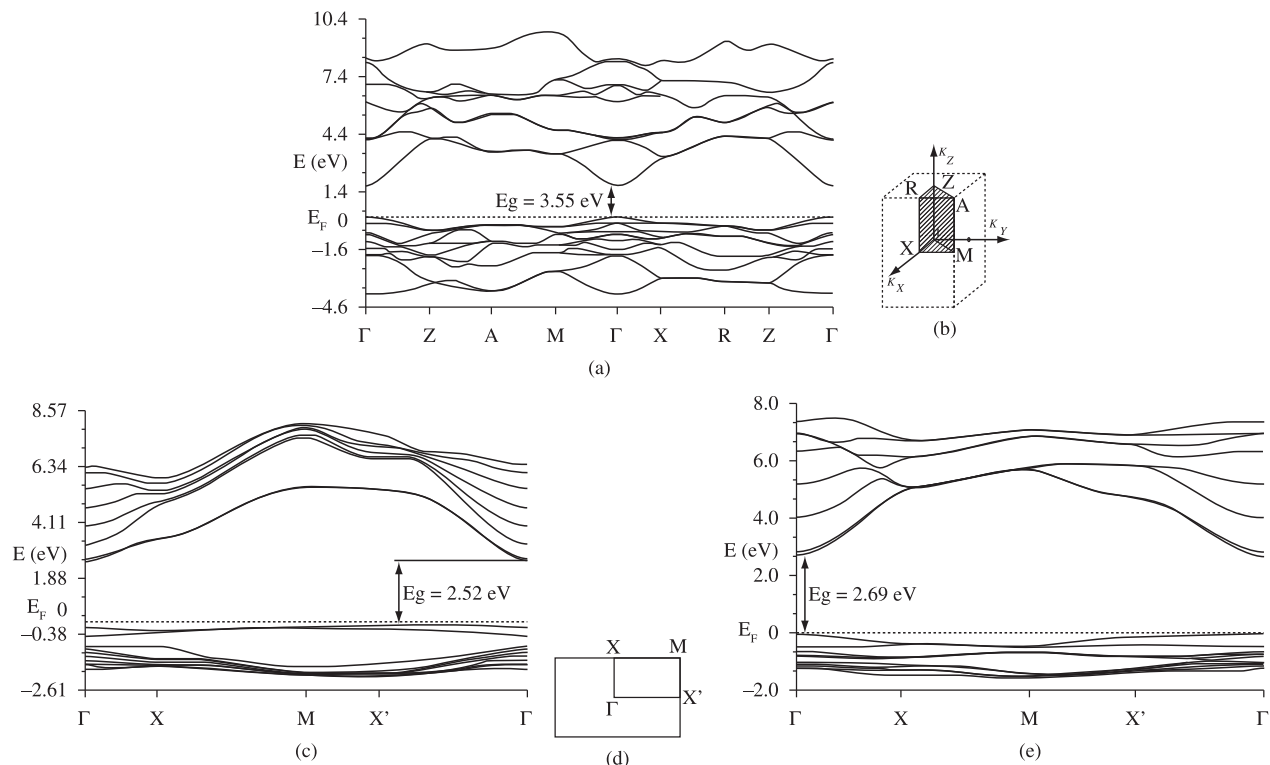


Figure 7. Calculated band structure diagram for SnO₂; a) bulk; c) surface (110); and e) surface (101). Brillouin Zone for SnO₂; b) bulk and d) Surface (110) and surface (101).

Figure 7c, 7d and 7e represents the band structure for surface (110), the high-symmetry paths of the adequate 2D Brillouin zone and the band structures for surface (101), respectively.

For the (110) surface the top of the upper valence band (VB) is located between X' and Γ points bottom of the lowest conduction band (CB) is located at Γ point. The gap becomes indirect and is reduced to 2.52 eV, compared with the bulk value. On the other hand, for the (101) surface, the energy gap is direct at Γ points, 2.69 eV, in good agreement with published data^{23,37}. The overall characteristics of the structural properties and electronic structure are coincident with previous investigations^{37,38}.

The data presented in this paper lead to some correlated interpretation as follows:

- 1) According to evaluation through Scherrer equation, films present nanoscopic dimensions crystallites and, as already mentioned, nanometric dimension particles in general, present the surface (101) as dominant^{20,23}.
- 2) Analysis of X-ray diffraction data also lead to a material with preferential growth in the (101) direction, which is consistent with the crystallites dimensions.
- 3) Results obtained from theoretical calculation of bulk and (101) surface yields direct band gap as the shortest transition.
- 4) Determination of band gap from electro-optical data (photoconductivity spectra) leads to fair values when the band gap nature is assumed as direct.

5. Conclusion

Sol-gel dip-coating SnO₂ thin films, deposited on quartz substrates, present (101) preferential growth direction and nanometric dimension crystallites. Theoretical evaluation of (101) surface along with bulk calculation leads to direct bandgap transition at Γ point. Evaluation of direct bandgap transition from optical absorption data yields 4.1eV.

Evaluation of direct transition bandgap from temperature dependent photoconductivity data yields 4.2 eV at room temperature, which decreases as the temperature is decreased. On the other hand, assuming indirect transition the calculation does not lead to physically acceptable result when the temperature is decreased

Band structure analysis of bulk and (101) surface in conjunction with experimental data of X-ray diffraction, optical absorption and photoconductivity, suggest that the experimental determination of bandgap in SnO₂ sol-gel-dip-coating thin films is related to combined effects of nanocrystallite dimensions and optical absorption of (101) surface and bulk, since both present direct bandgap.

Acknowledgements

Authors wish to thank Prof. Ligia O. Ruggiero by the equipment and Mr. Leandro P. Ravaro by all the help with the experimental setup. Authors also wish to express their gratitude to Brazilian financial agencies: CNPq and FAPESP.

References

1. Kong LB, Li FC, Zhang LY and Yao X. Sol-gel glasses coated zinc oxide as varistors. *Journal of Materials Science Letters*. 1998; 17(9):769-771.
2. Yang SL and Wu JM. Effects of Nb₂O₅ in (Ba, Bi, Nb)- added TiO₂ ceramic varistors. *Journal of Materials Research*. 1995; 10(2):345-352.
3. Wenas WW, Yamada A, Takahashi K, Yoshino M and Konagai M. Electrical and optical properties of boron-doped ZnO thin films for solar cells grown by metalorganic chemical vapour deposition. *Journal of Applied Physics*. 1991; 70(11):7119-7123.
4. Senguttuvan TD and Malhotra LK. Sol gel deposition of pure and antimony doped tin dioxide thin films by non alkoxide precursors. *Thin Solid Films*. 1996; 289(1-2):22-28.
5. Rai T, Senguttuvan TD and Lakshmi Kumar ST. Study of the electronic and optical bonding properties of doped SnO₂. *Computational Materials Science*. 2006; 37(1-2):15-19.
6. Serin T, Serin N, Karadeniz S, Sari H, Tugluoglu N and Pakma O. Electrical, structural and optical properties of SnO₂ thin films prepared by spray pyrolysis. *Journal of Non-Crystalline Solids*. 2006; 352(3):209-215.
7. Çetinörgü E, Goldsmith S and Boxman RL. Air annealing effects on the optical properties of ZnO-SnO₂ thin films deposited by a filtered vacuum arc deposition system. *Semiconductor Science and Technology*. 2006; 21(3):364-369.
8. Robertson J. Electronic Structure of SnO₂, GeO₂, PbO₂, TeO₂ and MgF₂. *Journal of Physics C: Solid State Physics*. 1979; 12(22):4767-4776.
9. Grieser F and Meisel D. Electron transfer in aqueous colloidal SnO₂ solutions. *Langmuir*. 1990; 6(3):567-572.
10. Gu Z, Liang P, Liu X, Zangh W and Le Y. Characteristics of Sol-Gel SnO₂ Films Treated by Ammonia. *Journal of Sol-Gel Science and Technology*. 2000; 18(2):159-166.
11. Jacquemin JL, Alibert C and De Murcia M. Electrotransmission Spectra of Stannic Oxide Single Crystals near the Fundamental Threshold. *Physica Status Solidi (B)*. 1972; 51(1):75-76.
12. Shanthi E, Dutta V, Banerjee A and Chopra KL. Electrical and optical properties of undoped and antimony-doped tin oxide films. *Journal of Applied Physics*. 1980; 51(12):6243-6251.
13. Messias FR, Vega BAV, Scalvi LVA, Siu Li M, Santilli CV and Pulcinelli SH. Electron scattering and effects of sources of light on photoconductivity of SnO₂ coatings prepared by sol-gel. *Journal of Non-Crystalline Solids*. 1999; 247(1):171-175.
14. Geraldo V, Scalvi LVA, Morais EA, Santilli CV, Miranda PB and Pereira TJ. Ultraviolet excitation of photoconductivity in thin films of sol-gel SnO₂. *Journal of the European Ceramic Society*. 2005; 25(12):2825-2828.
15. Martins JB, Taft CA, Longo E and Andres J. Ab initio study of CO and H₂ interaction on ZnO surfaces using a small cluster model. *Journal of Molecular Structure: Theochem*. 1997; 398:457-466.
16. Pacchioni G, Ferrari AM and Bagus PS. Cluster and band structure ab initio calculations on the adsorption of CO on acid sites of the TiO₂ (110) surface. *Surface Science*. 1996; 350(1-3):159-175.
17. Rantala TT, Rantala TS and Lantto V. Electronic structure of SnO₂ (110) surface. *Materials Science in Semiconductor Processing*. 2000; 3(1-2):103-107.
18. Mäki-Jaskari MA and Rantala TT. Band structure and optical parameters of the SnO₂ (110) surface. *Physical Review B*. 2001; 64(7):1-7.
19. Manassidis I, Goniakowski J, Kantorovich LN and Gillan MJ. The Structure of The Stoichiometric and Reduced SnO₂ (110) Surface. *Surface Science*. 1995; 339(3):258-271.
20. Batzill M and Diebold U. The surface and materials science of tin oxide. *Progress in Surface Science*. 2005; 79(2-4):47-154.
21. Godin TJ and Lafemina JP. Surface atomic and electronic structure of cassiterite SnO₂ (110). *Physical Review B*. 1993; 47(11):6518-6523.
22. Gunnarsson O, Satpathy S, Jepsen O and Andersen OK. Orientation of C₆₀ Cluster in Solids. *Physical Review Letters*. 1991; 67(21):3002-3005.
23. Katsiev K, Batzill M, Diebold U, Urban A and Meyer B. Growth of One-Dimensional Pd Nanowires on the Terraces of a Reduced SnO₂ (101) Surface. *Physical Review Letters*. 2007; 98(18):186102.
24. Khon W, Becke AD and Parr RG. Density Functional Theory of Electronic Structure. *The Journal of Physical Chemistry*. 1996; 100(31):12974-12980.
25. Becke AD. Density-functional thermochemistry. III. The role of exact exchange. *Journal of Chemical Physics*. 1993; 98(7):5648-5652.
26. Lee C, Yang W and Parr RG. Development of the Colle-Salvetti correlation-energy formula into a functional of the electron density. *Physical Review B*. 1988; 37(2):785-789.

27. Dovesi R, Saunders VR, Roetti C, Orlando R, Zicovich-Wilson CM, Pascale F et al. *CRYSTAL06 User's Manual*. University of Torino; 2006.
28. Muscat J, Wander A and Harrison NM. On the prediction of band gaps from hybrid functional theory. *Chemical Physics Letters*. 2001; 342(3-4):397-401.
29. Sambrano JR, Orhan E, Gurgel MFC, Campos AB, Goes MS, Paiva-Santos CO et al. Theoretical analysis of the structural deformation in Mn-doped BaTiO₃. *Chemical Physics Letters*. 2005; 402(4-6):491-496.
30. Sambrano JR, Longo VM, Longo E and Taft CA. Electronic and structural properties of the (001) SrZrO₃ surface. *Journal of Molecular Structure: Theochem*. 2007; 813(1-3):49-56.
31. De Lazaro SR, De Lucena PR, Sambrano JR, Pizani PS, Beltran A, Varela JA et al. Pb_{1-x}Ca_xTiO₃ solid solution (x=0.0, 0.25, 0.50, and 0.75): a theoretical and experimental approach. *Physical Review B*. 2007; 75(14):144111.
32. Theory of Condensed Matter Group. *Oxygen basis sets for the Crystal Program*. Available from: <http://www.tcm.phy.cam.ac.uk/~mdt26/basis_sets/O_basis.txt>.
33. Causa M, Dovesi R and Roetti C. Pseudopotential Hartree-Fock study of seventeen III-V and IV-IV semiconductors. *Physical Review B*. 1991; 43(14):11937-11943.
34. Durand Ph and Barthelat JC. A theoretical method to determine atomic pseudopotentials for electronic structure calculations of molecules and solids. *Theoretical Chemistry Accounts*. 1975; 38(4):283-302.
35. Munnix S and Schmeits M. Electronic structure of tin dioxide surfaces. *Physical Review B*. 1983; 27(12):7624-7635.
36. Batzill M, Chaka AM and Diebold U. Surface oxygen chemistry of a gas-sensing material: SnO₂ (101). *Europhysics Letters*. 2004; 65(1):61-67.
37. Beltrán A, Andrés J, Sambrano JR and Longo E. Density functional theory study on the structural and electronic properties of low index rutile surfaces for TiO₂/SnO₂/TiO₂ and SnO₂/TiO₂/SnO₂ composite systems. *The Journal of Physical Chemistry A*. 2008; 112(38):8943-8952.
38. Diebold U. The surface science of titanium dioxide. *Surface Science Reports*. 2003; 48(5-8):53-229.
39. Sensato FR, Custódio R, Calatayud M, Beltrán A, Andrés J, Sambrano JR et al. Periodic study on the structural and electronic properties of bulk, oxidized and reduced SnO₂(1 1 0) surfaces and the interaction with O₂. *Surface Science*. 2002; 511(1-3):408-420.
40. Kokalj A. XCrySDen - a new program for displaying crystalline structures and electron densities. *Journal of Molecular Graphics Modeling*. 1999; 17(3-4):176-179.
41. JCPDS- International Centre For Diffraction Data. 2003.
42. Cullity BD and Stock R. *Elements of X-Ray Diffraction*. 3th ed. New Jersey: Prentice Hall; 2001.
43. Moholkar AV, Pawar SM, Rajpure KY, Patil PS and Bhosale CH. Properties of highly oriented spray-deposited fluorine-doped tin oxide thin films on glass substrates of different thickness. *Journal of Physics and Chemistry of Solids*. 2007; 68(10):1981- 1988.
44. Sundaram KB and Bhagavat GK. Optical absorption studies on tin oxide films. *Journal of Physics D: Applied Physics*. 1981; 14(5):921-925.
45. Terrier C, Chatelon JP and Roger JA. Electrical and optical properties of Sb:SnO₂ thin films obtained by the sol-gel method. *Thin Solid Films*. 1997; 295(1-2):95-100.
46. De Souza AE, Monteiro SH, Santilli CV and Pulcinelli SH. Electrical and optical characteristics of SnO₂ thin films prepared by dip coating from aqueous colloidal suspensions. *Journal of Materials Science: Materials in Electronics*. 1997; 8(4):265-270.
47. Pankove IJ. *Optical Processes in Semiconductors*. New York: Dover Publications Inc; 1971.
48. Sze SM. *Semiconductor Devices, Physics & Technology*. 2nd ed. New York: John Wiley & Sons; 1985.
49. Mishra KC, Johnson KH and Schmidt PC. Electronic structure of antimony-doped tin oxide. *Physical Review B*. 1995; 51(20):13972-13976.